Supplementary Figures

Improved predictions of phase behaviour of intrinsically disordered proteins by tuning the interaction range

Giulio Tesei[1,*] and Kresten Lindorff-Larsen[1,*]

1 Structural Biology and NMR Laboratory & the Linderstrøm-Lang Centre for Protein Science, Department of Biology, University of Copenhagen, Copenhagen, Denmark

* giulio.tesei@bio.ku.dk, lindorff@bio.ku.dk

List of Figures

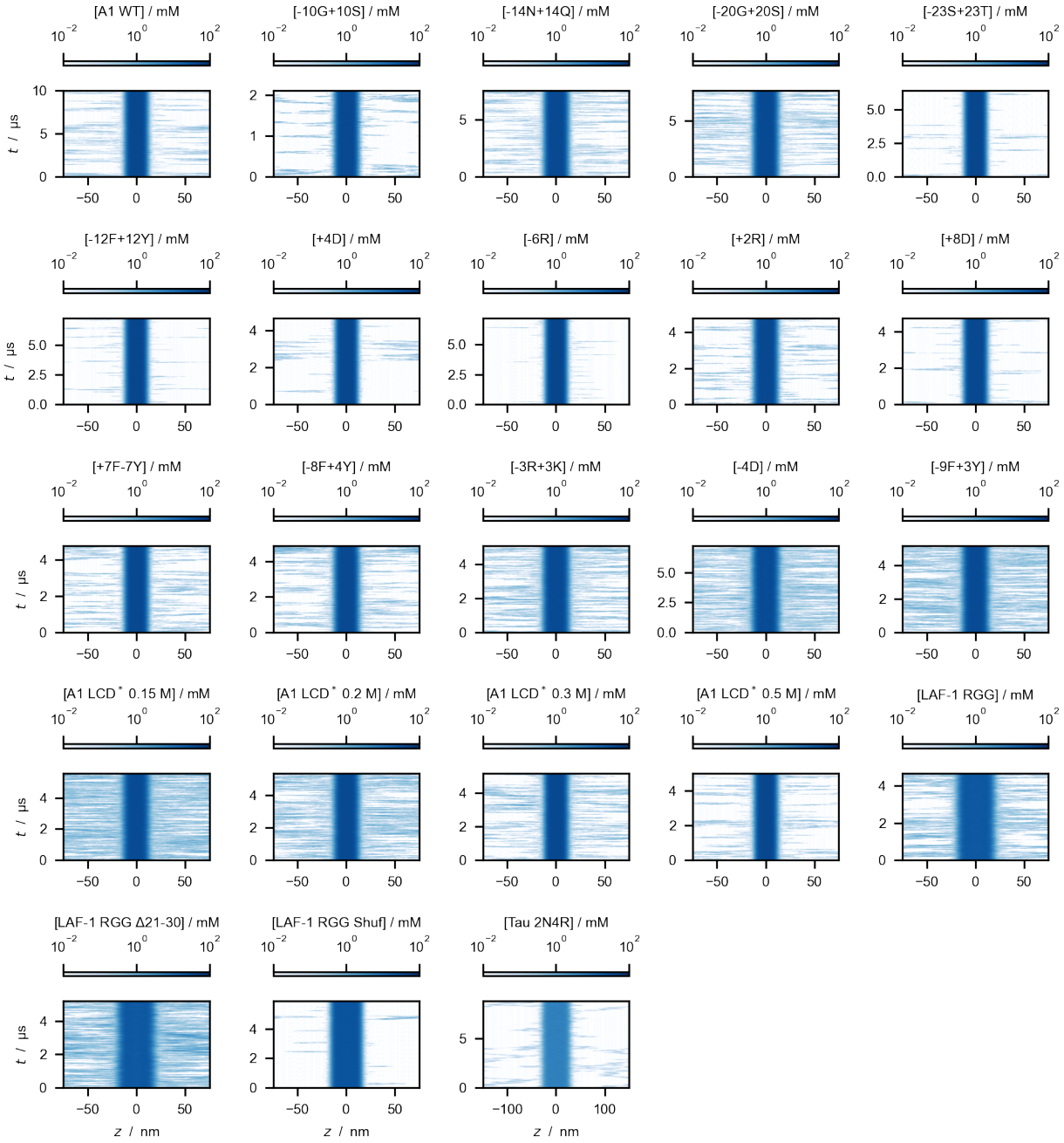

Figure S1: Time evolution of protein concentration along the z-axis of the simulation cell, as obtained from direct-coexistence simulations performed with the CALVADOS 1 model and $r_c = 4$ nm.

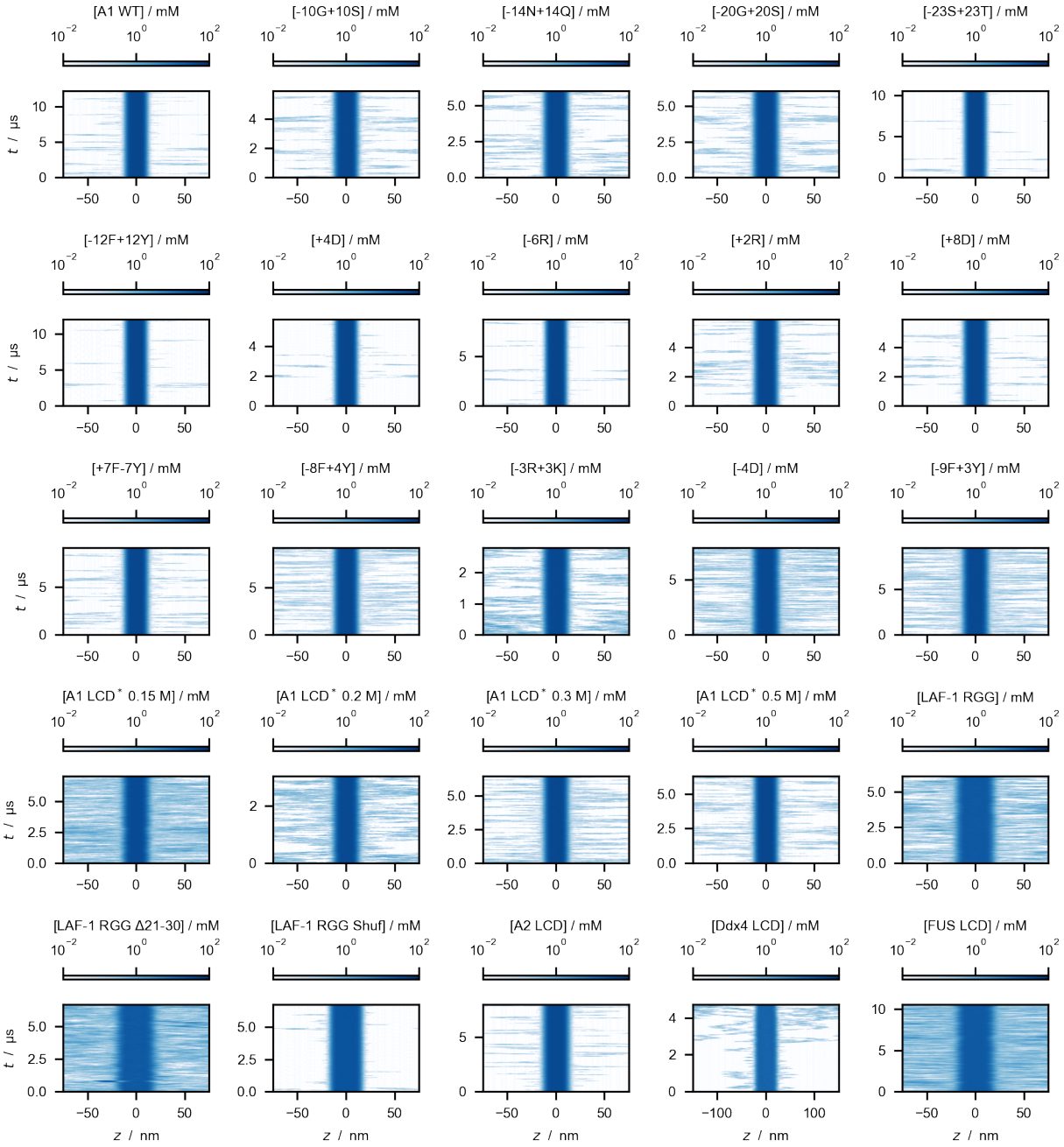

Figure S2: Time evolution of protein concentration along the z-axis of the simulation cell, as obtained from direct-coexistence simulations performed with the CALVADOS 1 model and $r_c = 2$ nm.

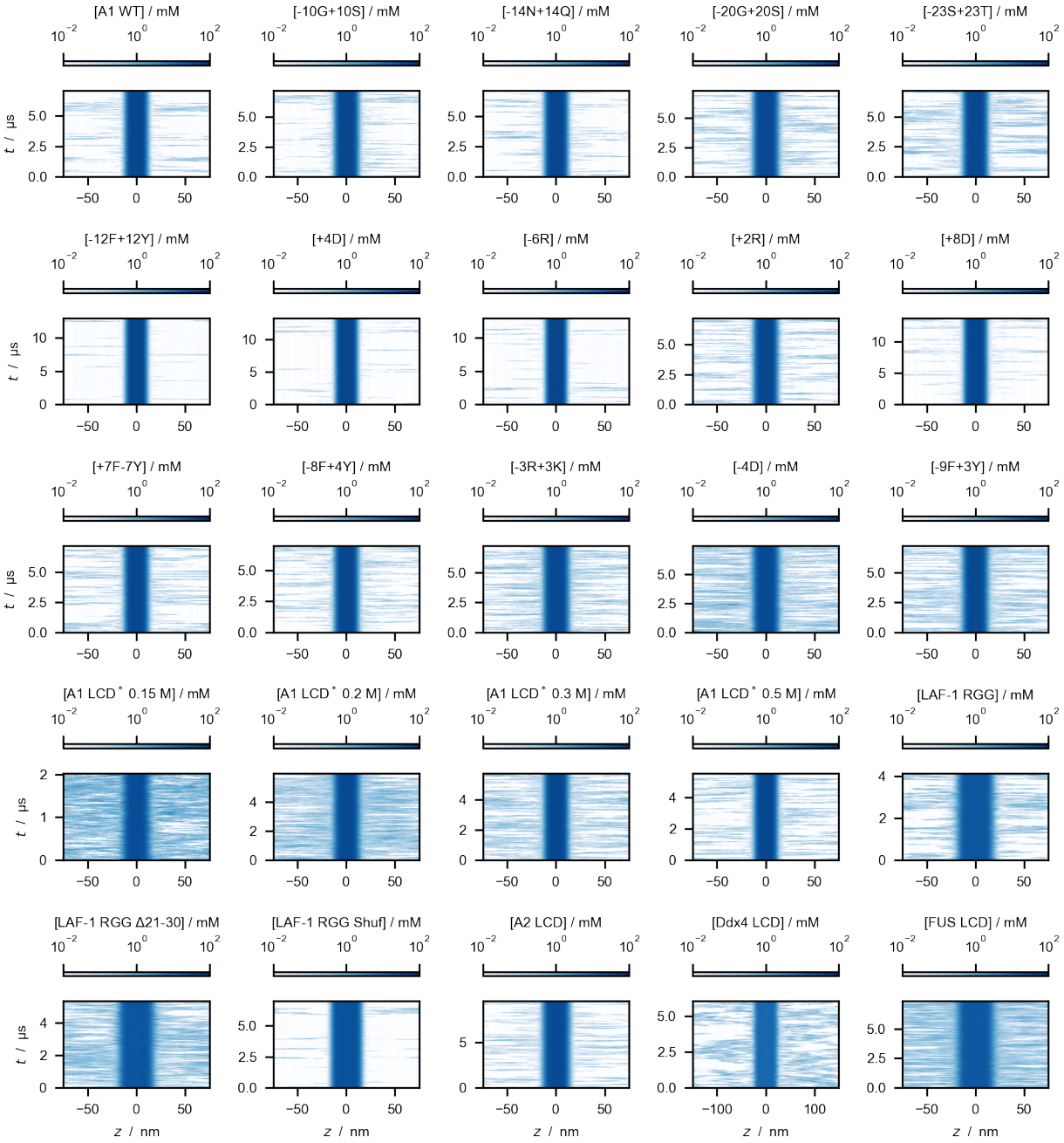

Figure S3: Time evolution of protein concentration along the z-axis of the simulation cell, as obtained from direct-coexistence simulations performed with the CALVADOS 2 model and $r_c = 2$ nm.

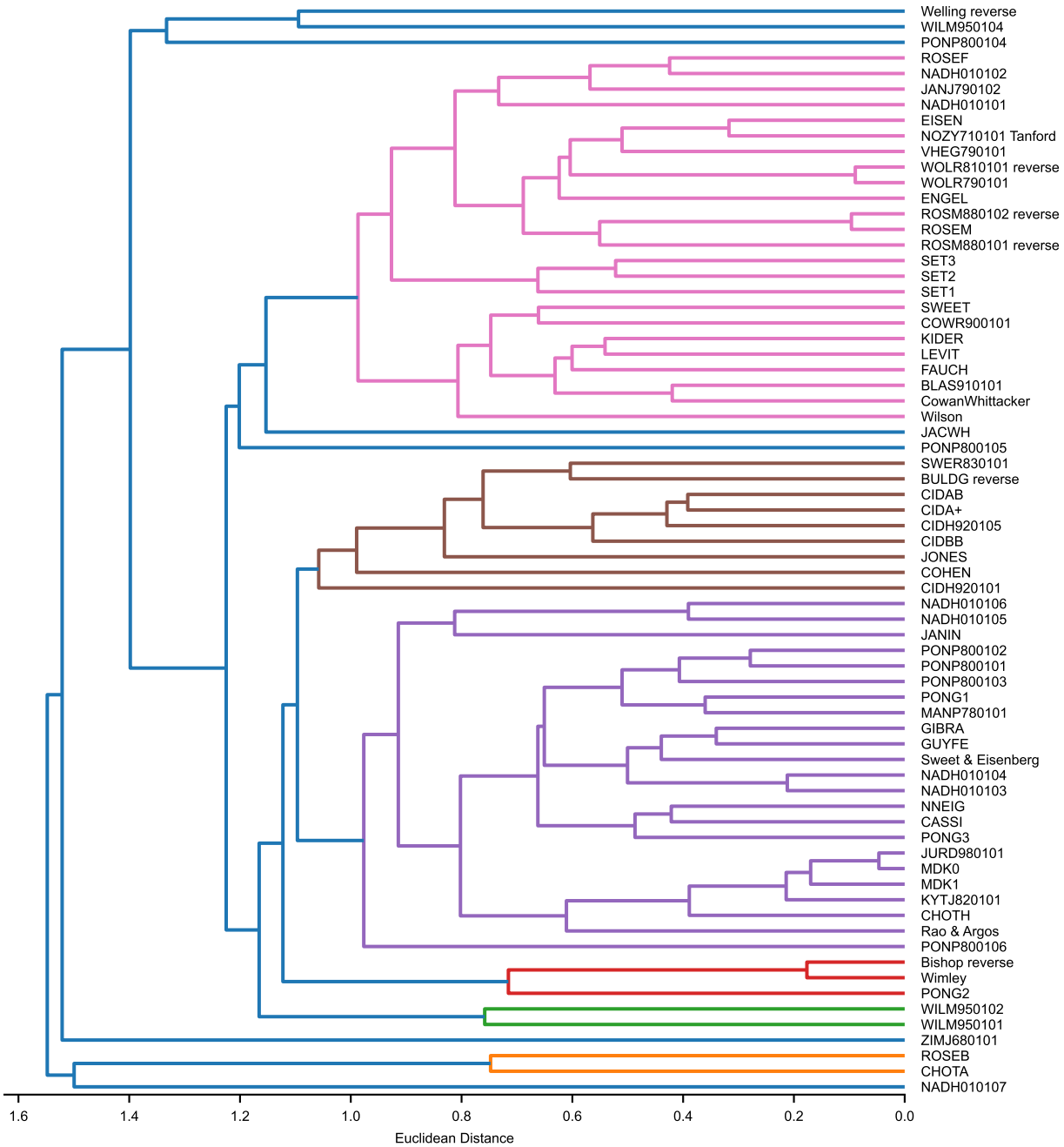

Figure S4: Hierarchical clustering dendrogram of 70 min-max normalized hydrophobicity scales selected from the set by Simm et al. [1]. Agglomerative clustering is performed using Euclidean distances and the average linkage method as implemented in the Python scikit-learn package [2].

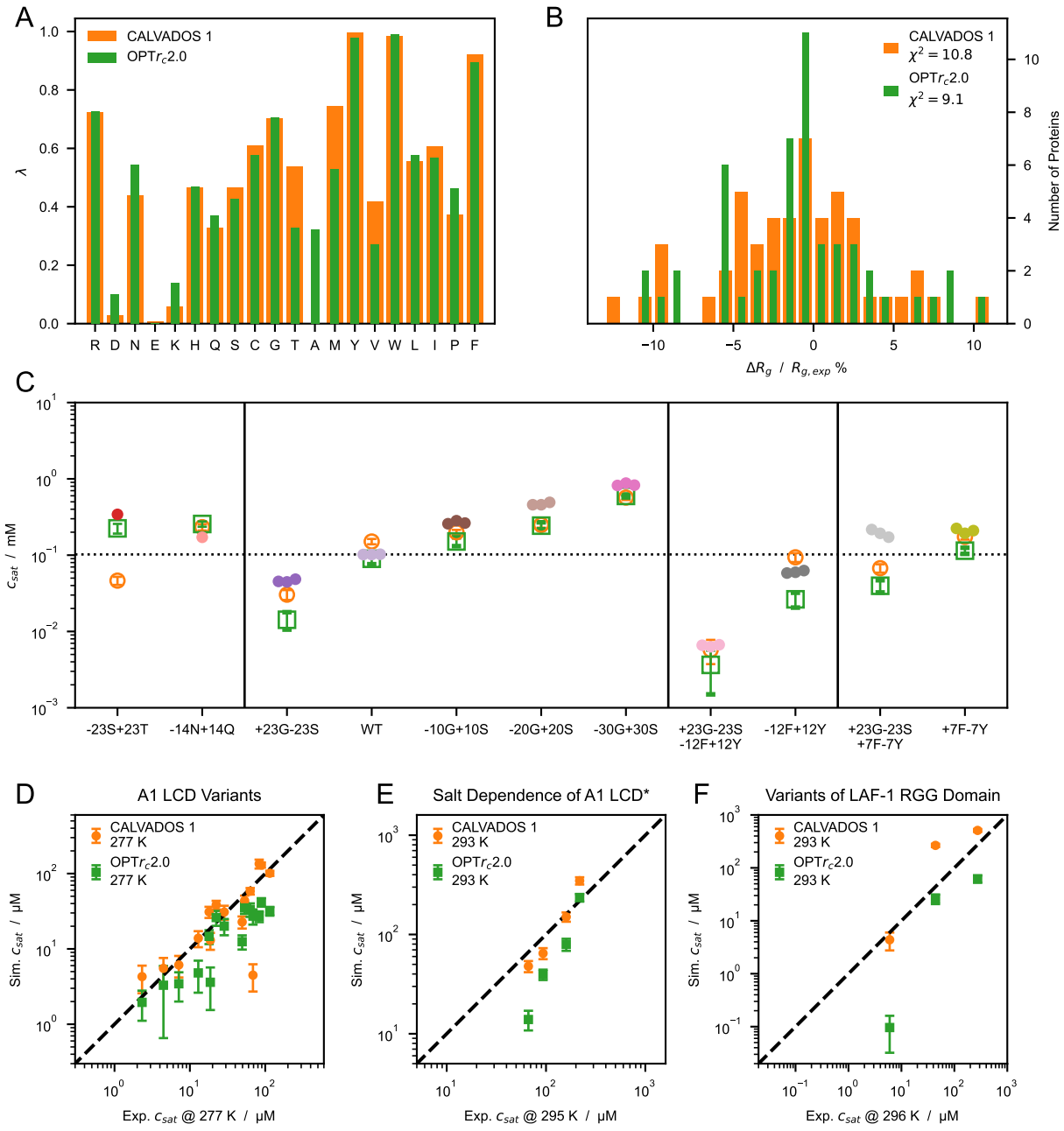

Figure S5: (*A*) Comparison between $\boldsymbol{\lambda}$ sets of CALVADOS 1 (orange) and the model resulting from the optimization with $r_c = 2.0$ nm (OPTr_c2.0, green). (*B*) Distribution of the relative difference between experimental (Table 1) and predicted radii of gyration, $\langle R_g \rangle$, for CALVADOS 1 (orange) and OPTr_c2.0 (blue). (*C*) Comparison between saturation concentrations, c_{sat}, at 293 K of variants of hnRNPA1 LCD measured by Bremer, Farag, Borcherds et al. [3] (closed circles) and corresponding predictions of CALVADOS 1 (open orange circles) and OPTr_c2.0 (open green squares). (*D–F*) Correlation between c_{sat} from simulations and experiments for (*D*) A1 LCD variants, (*E*) A1 LCD* WT at $[\mathrm{NaCl}] = 0.15$, 0.2, 0.3 and 0.5 M and (*F*) variants of LAF-1 RGG domain (Table 4).

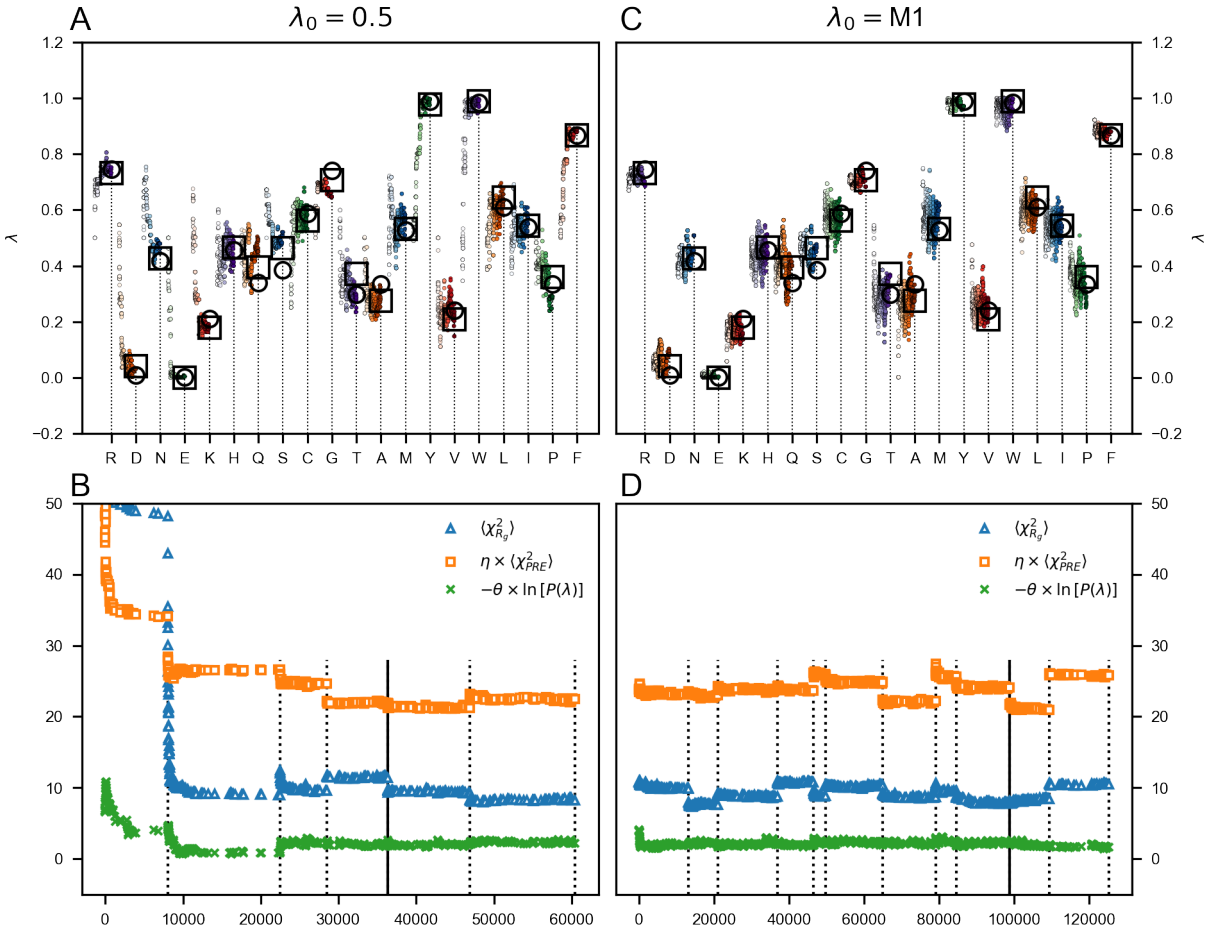

Figure S6: Optimization of the λ parameters starting from $\lambda_0 = 0.5$ (*A* and *B*) and λ_0 =M1 (*C* and *D*). (*A* and *B*) Evolution of the λ parameters during three consecutive optimization cycles. The color gradient from light to dark shade indicates increasing number of iterations. Open squares and circles show optimal λ sets obtained from indipendent optimizations starting from $\lambda_0 = 0.5$ and λ_0 =M1, respectively. (*C* and *D*) Evolution of $\chi 2_{R_g}$ (blue triangles), $0.1 \times \chi 2_{PRE}$ (orange squares), and the regularization term $0.05 \times \ln[P(\boldsymbol{\lambda})]$ (green circles). Dotted vertical lines indicate updated sampling by molecular simulations, whereas the remaining points are estimated from reweighted ensembles. Solid vertical lines indicate the optimal λ set corresponding to the lowest total cost function, $\mathcal{L}$.

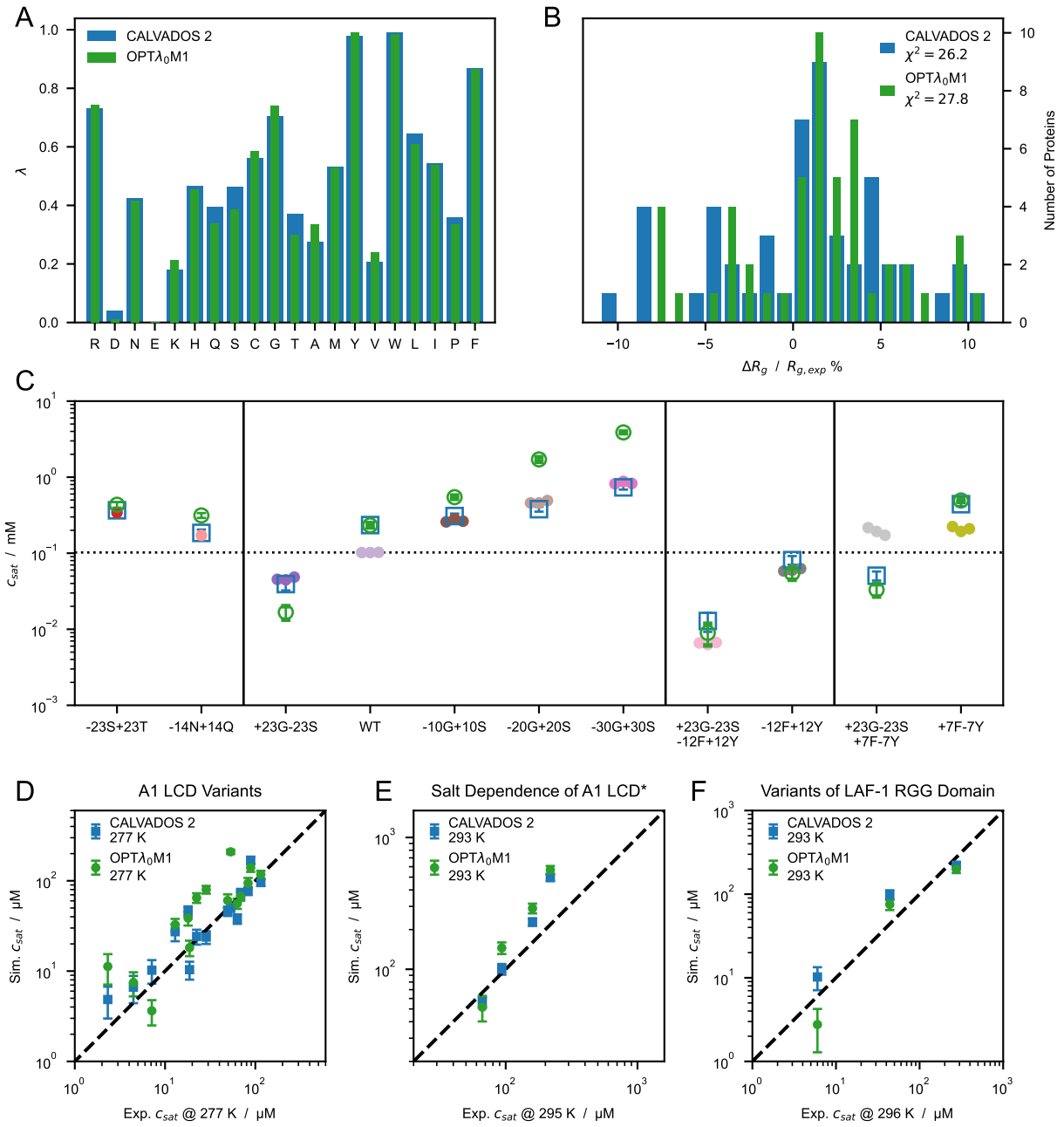

Figure S7: (*A*) Comparison between $\boldsymbol{\lambda}$ sets optimized starting from $\lambda_0 = 0.5$ (CALVADOS 2, blue) and λ_0 =M1 (OPTλ_0M1, green) using $r_c = 2.4$ nm. (*B*) Distribution of the relative difference between experimental (Table 1) and predicted radii of gyration, $\langle R_g \rangle$, for CALVADOS 2 (blue) and OPTλ_0M1 (green). (*C*) Comparison between saturation concentrations, c_{sat}, at 293 K of variants of hnRNPA1 LCD measured by Bremer, Farag, Borcherds et al. [3] (closed circles) and corresponding predictions of CALVADOS 2 (open blue squares) and OPTλ_0M1 (open green circles). (*D–F*) Correlation between c_{sat} from simulations and experiments for (*D*) A1 LCD variants, (*E*) A1 LCD* WT at $[\mathrm{NaCl}] = 0.15$, 0.2, 0.3 and 0.5 M and (*F*) variants of LAF-1 RGG domain (Table 4).

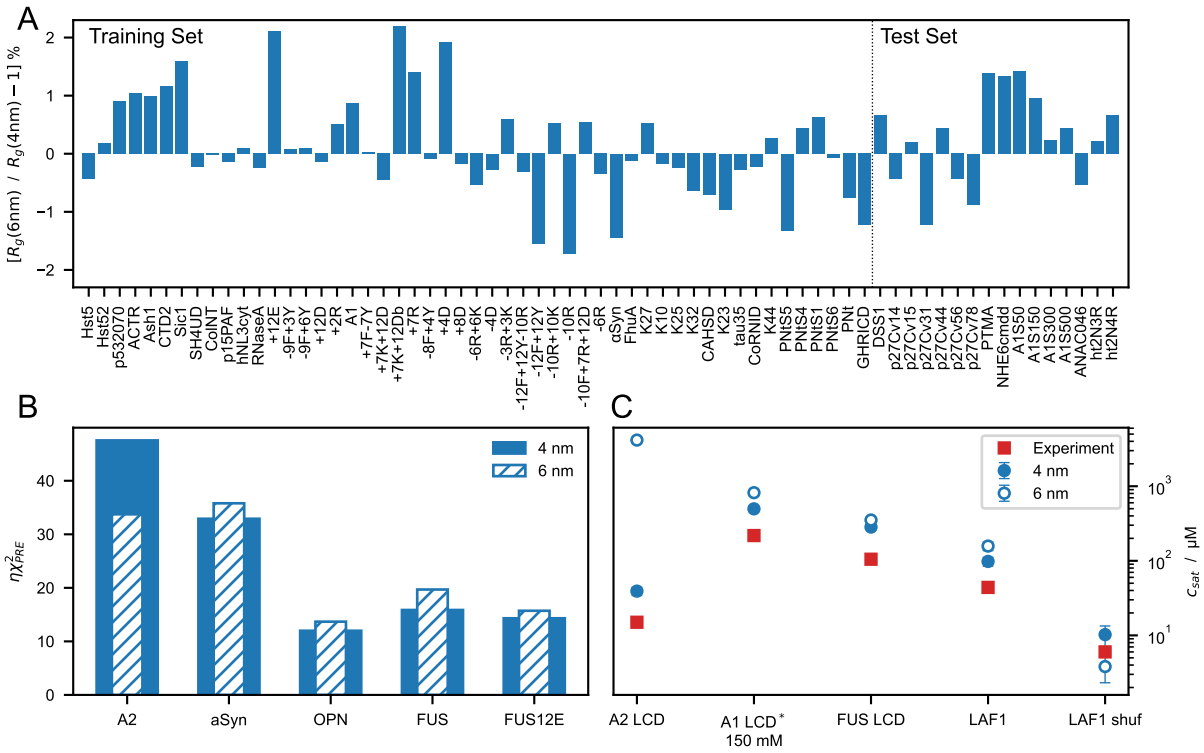

Figure S8: (A) Relative change in predicted R_g values upon increasing the cutoff for the ionic interactions from 4 to 6 nm. (B) Comparison between $\chi 2_{PRE}$ values for PRE data estimated from simulations performed using a cutoff of 4 (closed) and 6 nm (hatched) for the ionic interactions. (C) Comparison between experimental c_{sat} values (red squares) and predictions for A2 LCD ($c_s = 10$ mM), A1 LCD* ($c_s = 150$ mM), FUS LCD ($c_s = 150$ mM), LAF-1 RGG domain ($c_s = 150$ mM), and its shuffled variant ($c_s = 150$ mM) (Table 4) from simulations performed using a cutoff of 4 (closed blue circles) and 6 nm (open blue circles) for the ionic interactions.

Table 1: Solution conditions and experimental radii of gyration of proteins included in the training set for the Bayesian parameter-learning procedure.

Protein	N	R_g (nm)	T (K)	c_s (M)	pH	Ref.
Hst5	24	1.38 ± 0.05	293	0.15	7.5	[4]
$(Hst5)_2$	48	1.87 ± 0.05	298	0.15	7.0	[5]
p53 (20-70)	62	2.39 ± 0.05	277	0.1	7.0	[6]
ACTR	71	2.6 ± 0.1	278	0.2	7.4	[7]
Ash1	81	2.9 ± 0.05	293	0.15	7.5	[8, 9]
CTD2	83	2.61 ± 0.05	293	0.12	7.5	[10, 9]
Sic1	92	3.0 ± 0.4	293	0.2	7.5	[11]
SH4UD	95	2.7 ± 0.1	293	0.2	8.0	[12]
ColNT	98	2.8 ± 0.1	277	0.4	7.6	[13]
p15PAF	111	2.8 ± 0.1	298	0.15	7.0	[14]
hNL3cyt	119	3.2 ± 0.2	293	0.3	8.5	[15]
RNaseA	124	3.4 ± 0.1	298	0.15	7.5	[16]
A1	137	2.76 ± 0.02	298	0.15	7.0	[3]
-10R	137	2.67 ± 0.01	298	0.15	7.0	[3]
-6R	137	2.57 ± 0.01	298	0.15	7.0	[3]
+2R	137	2.62 ± 0.02	298	0.15	7.0	[3]
+7R	137	2.71 ± 0.01	298	0.15	7.0	[3]
-3R+3K	137	2.63 ± 0.02	298	0.15	7.0	[3]
-6R+6K	137	2.79 ± 0.01	298	0.15	7.0	[3]
-10R+10K	137	2.85 ± 0.01	298	0.15	7.0	[3]
+12D	137	2.80 ± 0.01	298	0.15	7.0	[3]
+4D	137	2.72 ± 0.03	298	0.15	7.0	[3]
+8D	137	2.69 ± 0.01	298	0.15	7.0	[3]
-9F+3Y	137	2.68 ± 0.01	298	0.15	7.0	[3]
+12E	137	2.85 ± 0.01	298	0.15	7.0	[3]
+7K+12D	137	2.92 ± 0.01	298	0.15	7.0	[3]
+7K+12D blocky	137	2.56 ± 0.01	298	0.15	7.0	[3]
-4D	137	2.64 ± 0.01	298	0.15	7.0	[3]
-8F+4Y	137	2.71 ± 0.01	298	0.15	7.0	[3]
-10F+7R+12D	137	2.86 ± 0.01	298	0.15	7.0	[3]
+7F-7Y	137	2.72 ± 0.01	298	0.15	7.0	[3]
-12F+12Y	137	2.60 ± 0.02	298	0.15	7.0	[3]
-12F+12Y-10R	137	2.61 ± 0.02	298	0.15	7.0	[3]
-9F+6Y	137	2.65 ± 0.01	298	0.15	7.0	[3]
αSyn	140	3.55 ± 0.1	293	0.2	7.4	[17]
FhuA	144	3.34 ± 0.1	298	0.15	7.5	[16]
K27	167	3.70 ± 0.2	288	0.15	7.4	[18]
K10	168	4.00 ± 0.1	288	0.15	7.4	[18]
K25	185	4.10 ± 0.2	288	0.15	7.4	[18]
K32	198	4.20 ± 0.3	288	0.15	7.4	[18]
CAHSD	227	4.8 ± 0.2	293	0.07	7.0	[19]
K23	254	4.9 ± 0.2	288	0.15	7.4	[18]
Tau35	255	4.7 ± 0.1	298	0.15	7.4	[20]
CoRNID	271	4.7 ± 0.2	293	0.2	7.5	[21]
K44	283	5.2 ± 0.2	288	0.15	7.4	[18]
PNt	334	5.1 ± 0.1	298	0.15	7.5	[16, 22]
PNt Swap1	334	4.9 ± 0.1	298	0.15	7.5	[22]
PNt Swap4	334	5.3 ± 0.1	298	0.15	7.5	[22]
PNt Swap5	334	4.9 ± 0.1	298	0.15	7.5	[22]
PNt Swap6	334	5.3 ± 0.1	298	0.15	7.5	[22]
GHRICD	351	6.0 ± 0.5	298	0.35	7.3	[23, 24]

Table 2: Solution conditions and experimental radii of gyration of proteins simulated in this study but not included in the training set for the Bayesian parameter-learning procedure.

Protein	N	R_g (nm)	T (K)	c_s (M)	pH	Ref.
DSS1	71	2.5 ± 0.1	288	0.17	7.4	[24]
p27Cv14	107	2.936 ± 0.13	293	0.095	7.2	[25]
p27Cv15	107	2.915 ± 0.10	293	0.095	7.2	[25]
p27Cv31	107	2.81 ± 0.18	293	0.095	7.2	[25]
p27Cv44	107	2.492 ± 0.13	293	0.095	7.2	[25]
p27Cv56	107	2.328 ± 0.10	293	0.095	7.2	[25]
p27Cv78	107	2.211 ± 0.03	293	0.095	7.2	[25]
PTMA	111	3.7 ± 0.2	288	0.16	7.4	[24]
NHE6cmdd	116	3.2 ± 0.2	288	0.17	7.4	[24]
A1 LCD*	131	2.645 ± 0.02	293	0.05	7.5	[26]
A1 LCD*	131	2.65 ± 0.02	293	0.15	7.5	[26]
A1 LCD*	131	2.62 ± 0.02	293	0.3	7.5	[26]
A1 LCD*	131	2.528 ± 0.02	293	0.5	7.5	[26]
ANAC046	167	3.6 ± 0.3	298	0.14	7.0	[24]
Tau 2N3R	410	6.3 ± 0.3	298	0.15	7.4	[20]
Tau 2N4R	441	6.7 ± 0.3	298	0.15	7.4	[20]

Table 3: Protein and conditions related to the intramolecular PRE data included in the training set.

Protein	N	N_{labels}	$\omega_I/2\pi$ (MHz)	T (K)	c_s (M)	pH	Ref.
FUS	163	3	850	298	0.15	5.5	[27]
FUS12E	164	3	850	298	0.15	5.5	[27]
OPN	220	10	800	298	0.15	6.5	[28]
αSyn	140	5	700	283	0.2	7.4	[29]
A2	155	2	850	298	0.005	5.5	[30]

Table 4: Proteins and conditions used for the direct-coexistence simulations performed in this study and references to the experimental data. Shaded rows highlight systems which are not included in the correlation plot of Figure 7*C*.

Protein	N	c_s (mM)	pH	Ref.	T (K)		
					4 nm	2 nm	Figure 3*D*
6His-TEV-Lge1$_{1-80}$-StrepII WT	114	100	7.5	[31]	-	293	-
6His-TEV-Lge1$_{1-80}$-StrepII -11R+11K	114	100	7.5	[31]	-	293	-
6His-TEV-Lge1$_{1-80}$-StrepII -14Y+14A	114	100	7.5	[31]	-	293	-
A1 LCD WT	137	150	7.0	[32, 3]	310 & 323	277 & 293	310
A1 LCD +7F-7Y	137	150	7.0	[3]	310 & 323	277 & 293	-
A1 LCD -12F+12Y	137	150	7.0	[3]	310 & 323	277 & 293	-
A1 LCD -23S+23T	137	150	7.0	[3]	310 & 323	277 & 293	-
A1 LCD -14N+14Q	137	150	7.0	[3]	310 & 323	277 & 293	-
A1 LCD -10G+10S	137	150	7.0	[3]	310 & 323	277 & 293	-
A1 LCD -20G+20S	137	150	7.0	[3]	310 & 323	277 & 293	-
A1 LCD -30G+30S	137	150	7.0	[3]	323	293	-
A1 LCD +23G-23S	137	150	7.0	[3]	323	293	-
A1 LCD +23G-23S+7F-7Y	137	150	7.0	[3]	323	293	-
A1 LCD +23G-23S-12F+12Y	137	150	7.0	[3]	323	293	-
A1 LCD -9F+3Y	137	150	7.0	[3]	310	277	-
A1 LCD -8F+4Y	137	150	7.0	[3]	310	277	-
A1 LCD -3R+3K	137	150	7.0	[3]	310	277	-
A1 LCD -6R	137	150	7.0	[3]	310	277	-
A1 LCD -4D	137	150	7.0	[3]	310	277	-
A1 LCD +4D	137	150	7.0	[3]	310	277	-
A1 LCD +8D	137	150	7.0	[3]	310	277	-
A1 LCD +2R	137	150	7.0	[3]	310	277	-
A1 LCD* WT	131	150	7.0	[33]	323	293	-
A1 LCD* WT	131	200	7.0	[33]	323	293	-
A1 LCD* WT	131	300	7.0	[33]	323	293	-
A1 LCD* WT	131	500	7.0	[33]	323	293	-
LAF-1 RGG Domain	176	150	7.5	[34]	323	293	293
LAF-1 RGG Domain Shuffled	176	150	7.5	[34]	323	293	323
LAF-1 RGG Domain Δ21-30	166	150	7.5	[34]	323	293	-
A2 LCD	155	10	5.5	[35]	-	297	-
FUS LCD	163	150	7.4	[36]	-	297	-
Ddx4 LCD	236	130	6.5	[37]	-	297	-
Human Full-Length Tau (2N4R)	441	70	7.4	-	-	-	277

Grant information

This project has received funding from the European Union's Horizon 2020 research and innovation programme under the Marie Skłodowska-Curie grant agreement No 101025063.

References

[1] Stefan Simm, Jens Einloft, Oliver Mirus, and Enrico Schleiff. 50 years of amino acid hydrophobicity scales: revisiting the capacity for peptide classification. *Biological Research*, 49(1), July 2016. doi:10.1186/s40659-016-0092-5.

[2] F. Pedregosa, G. Varoquaux, A. Gramfort, V. Michel, B. Thirion, O. Grisel, M. Blondel, P. Prettenhofer, R. Weiss, V. Dubourg, J. Vanderplas, A. Passos, D. Cournapeau, M. Brucher, M. Perrot, and E. Duchesnay. Scikit-learn: Machine learning in Python. *Journal of Machine Learning Research*, 12:2825–2830, 2011.

[3] Anne Bremer, Mina Farag, Wade M. Borcherds, Ivan Peran, Erik W. Martin, Rohit V. Pappu, and Tanja Mittag. Deciphering how naturally occurring sequence features impact the phase behaviours of disordered prion-like domains. *Nature Chemistry*, December 2021. doi:10.1038/s41557-021-00840-w.

[4] S. Jephthah, L. Staby, B. B. Kragelund, and M. Skepö. Temperature dependence of intrinsically disordered proteins in simulations: What are we missing? *Journal of Chemical Theory and Computation*, 15(4):2672–2683, March 2019. doi:10.1021/acs.jctc.8b01281.

[5] Eric Fagerberg, Linda K. Månsson, Samuel Lenton, and Marie Skepö. The effects of chain length on the structural properties of intrinsically disordered proteins in concentrated solutions. *The Journal of Physical Chemistry B*, 124(52):11843–11853, December 2020. doi:10.1021/acs.jpcb.0c09635.

[6] Jing Zhao, Alan Blayney, Xiaorong Liu, Lauren Gandy, Weihua Jin, Lufeng Yan, Jeung-Hoi Ha, Ashley J. Canning, Michael Connelly, Chao Yang, Xinyue Liu, Yuanyuan Xiao, Michael S. Cosgrove, Sozanne R. Solmaz, Yingkai Zhang, David Ban, Jianhan Chen, Stewart N. Loh, and Chunyu Wang. EGCG binds intrinsically disordered n-terminal domain of p53 and disrupts p53-MDM2 interaction. *Nature Communications*, 12(1), February 2021. doi:10.1038/s41467-021-21258-5.

[7] Magnus Kjaergaard, Ann–Beth Nørholm, Ruth Hendus–Altenburger, Stine F. Pedersen, Flemming M. Poulsen, and Birthe B. Kragelund. Temperature-dependent structural changes in intrinsically disordered proteins: Formation of α-helices or loss of polyproline II? *Protein Science*, 19(8):1555–1564, 2010. doi:https://doi.org/10.1002/pro.435.

[8] Erik W. Martin, Alex S. Holehouse, Christy R. Grace, Alex Hughes, Rohit V. Pappu, and Tanja Mittag. Sequence determinants of the conformational properties of an intrinsically disordered protein prior to and upon multisite phosphorylation. *Journal of the American Chemical Society*, 138(47):15323–15335, 2016. doi:10.1021/jacs.6b10272.

[9] Fan Jin and Frauke Gräter. How multisite phosphorylation impacts the conformations of intrinsically disordered proteins. *PLOS Computational Biology*, 17(5):e1008939, May 2021. doi:10.1371/journal.pcbi.1008939.

[10] Eric B. Gibbs, Feiyue Lu, Bede Portz, Michael J. Fisher, Brenda P. Medellin, Tatiana N. Laremore, Yan Jessie Zhang, David S. Gilmour, and Scott A. Showalter. Phosphorylation induces sequence-specific conformational

switches in the RNA polymerase II c-terminal domain. *Nature Communications*, 8(1), May 2017. doi:10.1038/ncomms15233.

[11] Gregory-Neal W. Gomes, Mickaël Krzeminski, Ashley Namini, Erik W. Martin, Tanja Mittag, Teresa Head-Gordon, Julie D. Forman-Kay, and Claudiu C. Gradinaru. Conformational ensembles of an intrinsically disordered protein consistent with NMR, SAXS, and single-molecule FRET. *Journal of the American Chemical Society*, 142(37):15697–15710, August 2020. doi:10.1021/jacs.0c02088.

[12] Utsab R. Shrestha, Puneet Juneja, Qiu Zhang, Viswanathan Gurumoorthy, Jose M. Borreguero, Volker Urban, Xiaolin Cheng, Sai Venkatesh Pingali, Jeremy C. Smith, Hugh M. O'Neill, and Loukas Petridis. Generation of the configurational ensemble of an intrinsically disordered protein from unbiased molecular dynamics simulation. *Proceedings of the National Academy of Sciences*, 116(41):20446–20452, September 2019. doi:10.1073/pnas.1907251116.

[13] Christopher L. Johnson, Alexandra S. Solovyova, Olli Hecht, Colin Macdonald, Helen Waller, J. Günter Grossmann, Geoffrey R. Moore, and Jeremy H. Lakey. The two-state prehensile tail of the antibacterial toxin colicin n. *Biophysical Journal*, 113(8):1673–1684, October 2017. doi:10.1016/j.bpj.2017.08.030.

[14] Alfredo De Biasio, Alain Ibáñez de Opakua, Tiago N. Cordeiro, Maider Villate, Nekane Merino, Nathalie Sibille, Moreno Lelli, Tammo Diercks, Pau Bernadó, and Francisco J. Blanco. p15paf is an intrinsically disordered protein with nonrandom structural preferences at sites of interaction with other proteins. *Biophysical Journal*, 106(4):865–874, February 2014. doi:10.1016/j.bpj.2013.12.046.

[15] Aviv Paz, Tzviya Zeev-Ben-Mordehai, Martin Lundqvist, Eilon Sherman, Efstratios Mylonas, Lev Weiner, Gilad Haran, Dmitri I. Svergun, Frans A.A. Mulder, Joel L. Sussman, and Israel Silman. Biophysical characterization of the unstructured cytoplasmic domain of the human neuronal adhesion protein neuroligin 3. *Biophysical Journal*, 95(4):1928–1944, August 2008. doi:10.1529/biophysj.107.126995.

[16] Joshua A. Riback, Micayla A. Bowman, Adam M. Zmyslowski, Catherine R. Knoverek, John M. Jumper, James R. Hinshaw, Emily B. Kaye, Karl F. Freed, Patricia L. Clark, and Tobin R. Sosnick. Innovative scattering analysis shows that hydrophobic disordered proteins are expanded in water. *Science*, 358(6360):238–241, October 2017. doi:10.1126/science.aan5774.

[17] Mustapha Carab Ahmed, Line K. Skaanning, Alexander Jussupow, Estella A. Newcombe, Birthe B. Kragelund, Carlo Camilloni, Annette E. Langkilde, and Kresten Lindorff-Larsen. Refinement of α-synuclein ensembles against SAXS data: Comparison of force fields and methods. *Frontiers in Molecular Biosciences*, 8, April 2021. doi:10.3389/fmolb.2021.654333.

[18] Efstratios Mylonas, Antje Hascher, Pau Bernadó, Martin Blackledge, Eckhard Mandelkow, and Dmitri I. Svergun. Domain conformation of tau protein studied by solution small-angle x-ray scattering. *Biochemistry*, 47(39):10345–10353, September 2008. doi:10.1021/bi800900d.

[19] Cherie Hesgrove, Kenny H. Nguyen, Sourav Biswas, Charles A. Childs, KC Shraddha, Bryan X. Medina, Vladimir Alvarado, Feng Yu, Shahar Sukenik, Marco Malferrari, Francesco Francia, Giovanni Venturoli, Erik W. Martin, Alex S. Holehouse, and Thomas C. Boothby. Tardigrade cahs proteins act as molecular swiss army knives to mediate desiccation tolerance through multiple mechanisms. *bioRxiv*, 2021. doi:10.1101/2021.08.16.456555.

[20] Chen Lyu, Stefano Da Vela, Youssra Al-Hilaly, Karen E. Marshall, Richard Thorogate, Dmitri Svergun, Louise C. Serpell, Annalisa Pastore, and Diane P. Hanger. The disease associated tau35 fragment has an increased propensity to aggregate compared to full-length tau. *Frontiers in Molecular Biosciences*, 8, 2021. doi:10.3389/fmolb.2021.779240.

[21] Tiago N. Cordeiro, Nathalie Sibille, Pierre Germain, Philippe Barthe, Abdelhay Boulahtouf, Fréderic Allemand, Rémy Bailly, Valérie Vivat, Christine Ebel, Alessandro Barducci, William Bourguet, Albane le Maire, and Pau Bernadó. Interplay of protein disorder in retinoic acid receptor heterodimer and its corepressor regulates gene expression. *Structure*, 27(8):1270–1285.e6, August 2019. doi:10.1016/j.str.2019.05.001.

[22] Micayla A. Bowman, Joshua A. Riback, Anabel Rodriguez, Hongyu Guo, Jun Li, Tobin R. Sosnick, and Patricia L. Clark. Properties of protein unfolded states suggest broad selection for expanded conformational ensembles. *Proceedings of the National Academy of Sciences*, 117(38):23356–23364, September 2020. doi:10.1073/pnas.2003773117.

[23] Pernille Seiffert, Katrine Bugge, Mads Nygaard, Gitte W Haxholm, Jacob H Martinsen, Martin N Pedersen, Lise Arleth, Wouter Boomsma, and Birthe B Kragelund. Orchestration of signaling by structural disorder in class 1 cytokine receptors. *Cell Communication and Signaling*, 18(1):1–30, 2020.

[24] Francesco Pesce, Estella A. Newcombe, Pernille Seiffert, Emil E. Tranchant, Johan G. Olsen, Birthe B. Kragelund, and Kresten Lindorff-Larsen. Assessment of models for calculating the hydrodynamic radius of intrinsically disordered proteins. *bioRxiv*, 2022. doi:10.1101/2022.06.11.495732.

[25] Rahul K. Das, Yongqi Huang, Aaron H. Phillips, Richard W. Kriwacki, and Rohit V. Pappu. Cryptic sequence features within the disordered protein p27$^{\mathrm{Kip1}}$ regulate cell cycle signaling. *Proceedings of the National Academy of Sciences*, 113(20):5616–5621, May 2016. doi:10.1073/pnas.1516277113.

[26] Erik W Martin, F Emil Thomasen, Nicole M Milkovic, Matthew J Cuneo, Christy R Grace, Amanda Nourse, Kresten Lindorff-Larsen, and Tanja Mittag. Interplay of folded domains and the disordered low-complexity domain in mediating hnRNPA1 phase separation. *Nucleic Acids Research*, 49(5):2931–2945, February 2021. doi:10.1093/nar/gkab063.

[27] Zachary Monahan, Veronica H Ryan, Abigail M Janke, Kathleen A Burke, Shannon N Rhoads, Gül H Zerze, Robert O'Meally, Gregory L Dignon, Alexander E Conicella, Wenwei Zheng, Robert B Best, Robert N Cole, Jeetain Mittal, Frank Shewmaker, and Nicolas L Fawzi. Phosphorylation of the FUS low-complexity domain disrupts phase separation, aggregation, and toxicity. *The EMBO Journal*, 36(20):2951–2967, August 2017. doi:10.15252/embj.201696394.

[28] D. Kurzbach, A. Vanas, A. G. Flamm, N. Tarnoczi, G. Kontaxis, N. Maltar-Strmečki, K. Widder, D. Hinderberger, and R. Konrat. Detection of correlated conformational fluctuations in intrinsically disordered proteins through paramagnetic relaxation interference. *Physical Chemistry Chemical Physics*, 18(8):5753–5758, 2016. doi:10.1039/c5cp04858c.

[29] Matthew M. Dedmon, Kresten Lindorff-Larsen, John Christodoulou, Michele Vendruscolo, and Christopher M. Dobson. Mapping long-range interactions in α-synuclein using spin-label NMR and ensemble molecular dynamics simulations. *Journal of the American Chemical Society*, 127(2):476–477, January 2005. doi:10.1021/ja044834j.

[30] Veronica H. Ryan, Gregory L. Dignon, Gül H. Zerze, Charlene V. Chabata, Rute Silva, Alexander E. Conicella, Joshua Amaya, Kathleen A. Burke, Jeetain Mittal, and Nicolas L. Fawzi. Mechanistic view of hnRNPA2 low-complexity domain structure, interactions, and phase separation altered by mutation and arginine methylation. *Molecular Cell*, 69(3):465–479.e7, February 2018. doi:10.1016/j.molcel.2017.12.022.

[31] Anton A. Polyansky, Laura D. Gallego, Roman G. Efremov, Alwin Köhler, and Bojan Zagrovic. Protein compactness and interaction valency define the architecture of a biomolecular condensate across scales. *bioRxiv*, 2022. doi:10.1101/2022.02.18.481017.

[32] Erik W. Martin, Alex S. Holehouse, Ivan Peran, Mina Farag, J. Jeremias Incicco, Anne Bremer, Christy R. Grace, Andrea Soranno, Rohit V. Pappu, and Tanja Mittag. Valence and patterning of aromatic residues determine the phase behavior of prion-like domains. *Science*, 367(6478):694–699, February 2020. doi:10.1126/science.aaw8653.

[33] Erik W. Martin, Tyler S. Harmon, Jesse B. Hopkins, Srinivas Chakravarthy, J. Jeremías Incicco, Peter Schuck, Andrea Soranno, and Tanja Mittag. A multi-step nucleation process determines the kinetics of prion-like domain phase separation. *Nature Communications*, 12(1), July 2021. doi:10.1038/s41467-021-24727-z.

[34] Benjamin S. Schuster, Gregory L. Dignon, Wai Shing Tang, Fleurie M. Kelley, Aishwarya Kanchi Ranganath, Craig N. Jahnke, Alison G. Simpkins, Roshan Mammen Regy, Daniel A. Hammer, Matthew C. Good, and Jeetain Mittal. Identifying sequence perturbations to an intrinsically disordered protein that determine its phase-separation behavior. *Proceedings of the National Academy of Sciences*, 117(21):11421–11431, May 2020. doi:10.1073/pnas.2000223117.

[35] Veronica H Ryan, Theodora M Perdikari, Mandar T Naik, Camillo F Saueressig, Jeremy Lins, Gregory L Dignon, Jeetain Mittal, Anne C Hart, and Nicolas L Fawzi. Tyrosine phosphorylation regulates hnRNPA2 granule protein partitioning and reduces neurodegeneration. *The EMBO Journal*, 40(3), December 2020. doi:10.15252/embj.2020105001.

[36] Anastasia C. Murthy, Gregory L. Dignon, Yelena Kan, Gül H. Zerze, Sapun H. Parekh, Jeetain Mittal, and Nicolas L. Fawzi. Molecular interactions underlying liquid-liquid phase separation of the FUS low-complexity domain. *Nature Structural & Molecular Biology*, 26(7):637–648, July 2019. doi:10.1038/s41594-019-0250-x.

[37] Jacob P. Brady, Patrick J. Farber, Ashok Sekhar, Yi-Hsuan Lin, Rui Huang, Alaji Bah, Timothy J. Nott, Hue Sun Chan, Andrew J. Baldwin, Julie D. Forman-Kay, and Lewis E. Kay. Structural and hydrodynamic properties of an intrinsically disordered region of a germ cell-specific protein on phase separation. *Proceedings of the National Academy of Sciences*, 114(39):E8194–E8203, September 2017. doi:10.1073/pnas.1706197114.